Research Article

Dezhi Yang, Sohail Ahmad, Kashif Ali, Salem Algarni, Talal Alqahtani, Wasim Jamshed*, Syed M. Hussain, Kashif Irshad, and Hijaz Ahmad

CFD analysis of paraffin-based hybrid (Co–Au) and trihybrid (Co–Au–ZrO_2) nanofluid flow through a porous medium

https://doi.org/10.1515/ntrev-2024-0024
received October 2, 2023; accepted April 8, 2024

Abstract: Ternary hybrid nanofluids possess improved thermal characteristics, enhanced stability, better physical strength, and multi-functionality as compared to hybrid or usual nanofluids. The aim of the ongoing study is to explore the novel thermal attributes of hybrid and trihybrid nanofluids through a porous medium. Whereas the nano-composition of cobalt (Co), gold (Au), and zirconium oxide (ZrO_2) make amalgamation in the paraffin (Pfin) which is a base fluid. This nano-composition of the proposed nanoparticles, specifically, subject to the base fluid Pfin has not been interpreted before. The analysis not only covers the features of trihybrid nanofluids (Co–Au–ZrO_2–Pfin) but it also describes the characteristics of hybrid (Co–Au–Pfin) as well as pure nanofluids (Co–Pfin). An efficient numerical algorithm is developed for which the numerical simulations are carried out. The approximations are performed in MATLAB software using "Successive under Relaxation (SUR)" technique. A comparison, under certain limiting conditions, with the established results appraises the efficiency of the numerical code. The outcomes evidently designate that temperature raises with the change in thermal radiation and volume fraction of gold and zirconium oxide in either case of pure, hybrid, or ternary nanofluids. The concentration ϕ_3 of ZrO_2 has a significant impact on Nusselt number rather than the concentration ϕ_1 of cobalt and ϕ_2 of gold. It has been comparatively noticed that the ternary nanofluids (Co–Au–ZrO_2–Pfin) portray embellished and improvised thermal characteristics as compared to the other two cases.

Keywords: zirconium oxide, cobalt, gold, ternary hybrid nanofluids, paraffin, porous medium, SUR technique

*** Corresponding author: Wasim Jamshed,** Department of Mathematics, Capital University of Science and Technology (CUST), Islamabad 44000, Pakistan; Mathematics in Applied Sciences and Engineering Research Group, Scientific Research Center, Al-Ayen University, Nasiriyah 64001, Iraq, e-mail: wasiktk@hotmail.com
Dezhi Yang: College of Science, Qingdao University of Technology, Linyi, Shandong Province, China
Sohail Ahmad, Kashif Ali: Department of Basic Sciences and Humanities, Muhammad Nawaz Sharif University of Engineering and Technology, Multan 60000, Pakistan
Salem Algarni, Talal Alqahtani: Mechanical Engineering Department, College of Engineering, King Khalid University, Abha 9004, Saudi Arabia
Syed M. Hussain: Department of Mathematics, Faculty of Science, Islamic University of Madinah, Medina 42351, Saudi Arabia
Kashif Irshad: Interdisciplinary Research Centre for Sustainable Energy Systems (IRC-SES), Research Institute, King Fahd University of Petroleum and Minerals (KFUPM), Dhahran 31261, Saudi Arabia
Hijaz Ahmad: Department of Mathematics, Faculty of Science, Islamic University of Madinah, Medina 42351, Saudi Arabia; Near East University, Operational Research Center in Healthcare, TRNC Mersin 10, Nicosia 99138, Turkey; Center for Applied Mathematics and Bioinformatics, Gulf University for Science and Technology, Mishref, Kuwait; Department of Computer Science and Mathematics, Lebanese American University, Beirut, Lebanon

1 Introduction

The fluids that are engineered in such a way that the solid fragments of metallic or non-metallic materials are dispersed in the base fluids can be referred to as the nanofluids. These fluids have the capacity to embellish the thermal conductivity of host liquids, and this particular property makes them considerable in several scientific zones. An enhancement in the thermal and physical properties of base fluids are due to the nanofluids [1–5]. The amalgamation of three distinct nanoparticles into the base liquids gives rise to the ternary case of nanofluids and this mixture is called trihybrid or ternary hybrid nanofluids. Using several kinds of nanoparticles, ternary hybrid nanofluids offer a framework for designing nanofluid properties, opening new opportunities for improved thermal, mechanical, and electrical capabilities in a variety of applications. Some potential utilizations of ternary, mono, and hybrid nanofluids are as follows: electronics cooling to

reduce the risk of overheating [6]; solar thermal collectors by enhancing the absorption of solar radiation [7,8]; heat transfer enhancement in cooling systems, electronic devices, and heat exchangers (Panduro and Finotti [9]); and use in biomedical sciences like cancer therapy, tissue engineering and drug delivery [10,11]. The further prominent applications involve lubricants, engine cooling, oil recovery, and nuclear reactor cooling.

The current work reveals the novel features of three distinct nanoparticles, *e.g.*, cobalt, gold, and zirconium oxide which combined make ternary hybrid nanofluids Co–Au–ZrO_2/Pfin. Cobalt is a silvery-blue lustrous metal. It exhibits magnetic features, and is widely used in the preparation of magnets. Cobalt can produce power magnets when alloyed with nickel and aluminum. The recent uses of radioactive cobalt involve cancer treatment and food preservation. The other uses of cobalt alloys are jet and gas turbine generators, electroplating, and resistance to corrosion, and cobalt salt produces blue colors in pottery, glass, and paint. The cobalt, subject to different perspectives, has been investigated by several researchers. Rahman Salari [12] synthesized the tin dioxide (SnO_2) and cobalt oxide (CO_3) in the preparation of water-based nanofluid. They characterized the structural mechanism of nanoparticles by scanning, X-Ray diffraction, and Fourier transformation infrared spectroscopy. An investigation into the cobalt-based nanofluid with a concentration of 0.1–0.41 % was presented by Sekhar *et al.* [13]. The major aim, of their research, was to measure the conductivity of fluid as well as relative viscosity over a 30–60°C temperature range limit. Farooq *et al.* [14] comparatively analyzed the hybrid nanofluids Ag-$COFe_2O_4$ composed of silver and cobalt ferrite in the coexistence of magnetic field. Mathematical investigations were performed by Murtaza *et al.* [15] which incorporates the cobalt particles to synthesize the nanofluid with the impact of second-order slip and variable viscosity. Santhosh and Sivaraj [16] anticipated a hydro-magnetic flow inside a porous enclosure with mixed convective heat transfer. The enclosure contained base fluid (kerosene oil) and the ferromagnetic cobalt particles. Their results spotted that the blade-shaped cobalt nanoparticles had better effect on the heat transfer rather than the spherical-shaped cobalt nanoparticles. Mandal *et al.* [17] and Biswas *et al.* [18,19] examined the bio-convective flows through porous medium.

Gold is a chemical element and a precious metal having the symbol Au. In pure or natural form, it is a malleable, soft, dense, bright, ductile, and yellow-colored metal. In ancient times, gold was used as currency in the form of coins. Most of the gold in the world (78%) is used in jewelry. It is also used in electronics, medicine, and dentistry. Gold is most dense than all metals and good conductor of electricity as well as heat. The use of gold, in the thermal analysis, is found in many studies. Tsai *et al.* [20] analyzed various sized gold nanoparticles in an aqueous solution inside a circular heat pipe. The thermal resistance was noted to vary in the pipe with the change in the gold size of nanomaterial. The blood-based heat transfer micropolar nanofluid flow involving gold as nanoparticles was speculated by Khan *et al.* [21]. Several effects like microorganisms, Brownian motion, and chemically reactive activation energy were taken into consideration. Numerical studies of gold/water nanofluid and gold/blood nanofluid flow over a disk and within a permeable channel were studied by Magodora *et al.* [22] and Srinivas *et al.* [23], respectively. The work of Burgos *et al.* [24] described a statistical and experimental analysis of the gold nanoparticles on nanofluids stability and photothermal properties of the solar nanofluids.

The fusion-reduction process of zircon sand (zirconium silicate) gives rise to zirconia which is also recognized as zirconium di-oxide ZrO_2. The ceramic industry encompasses the potential employments of ZrO_2. This metal is inorganic in nature with better thermal and corrosion resistance, high refractory, and strong chemical inertness but low solubility and biocompatibility. Some recent investigations based on ZrO_2 nanoparticles can be studied in various research works [25–29].

The ternary hybrid nanofluids subject to different physical conditions have been examined recently by the research community. Shao *et al.* [30] investigated the natural convection phenomenon inside a prismatic porous enclosure filled with ternary hybrid nanofluid having two hot movable baffles. The simulations were performed to look into the effects of length between baffles and Darcy number on the thermal characteristics of trihybrid nanofluids. Some limitations in the mono nanofluids and advantages of the ternary hybrid nanofluids were pointed out by Adun *et al.* [31] in a review analysis of ternary hybrid nanofluids. In their analysis, they discussed the heat transfer characteristics, thermophysical properties, stability, and synthesis of ternary hybrid nanofluids. Algehyne *et al.* [32] used the non-Fourier's concept and variable diffusion to numerically elaborate the trihybrid nanofluids involving nanoparticles of magnesium oxide (MgO), cobalt ferrite ($CoFe_2O_4$), and titanium dioxide (TiO_2). Their results spotted that hybrid and trihybrid case of nanofluids had a better efficiency for velocity propagation rate and fluid energy. The usages of three different types of nanoparticles (trihybrid case) and their importance in heat transport rate subject to dynamics of coolant in automobiles and fuel were prescribed by Elnaqeeb *et al.* [33]. The ternary nanofluid

Table 1: Some recent studies consisting of several trihybrid nanoparticles

References	Nanoparticles	Base fluid	Prominent effects
Abeer *et al.* [46]	TiO_2–CuO–Al_2O_3	Blood	Ohmic heat, energy emission/absorption, nonlinear thermal radiation
Yaseen *et al.* [47]	CNT–Cu–Al_2O_3	Water	Second-degree thermal radiation, magnetic field
Cao *et al.* [48]	CNTs–Go–Al	Ethylene glycol	Mixed convection, partial slip
Noreen *et al.* [49]	SiO_2–Fe_3O_4–Cu	Kerosene oil	Magnetohydrodynamics
Nabwey *et al.* [50]	Ag–TiO_2–Al_2O_3	Water	Magnetic field, radiative heat flux

was prepared using the nano-composition of Ag–TiO_2–Cu/water (Li *et al.* [34]). Some prominent effects like temperature jump and Troian and Thomson slip conditions were considered in the model problem. The RKF-45 methodology was incorporated to determine the approximate solution of the problems. It was examined (in this research) that the flow speed got reduced by the slip in the velocity. The recent works [35–45] further interpret the relevant studies. Some recent studies consisting of several trihybrid nanoparticles are portrayed in Table 1.

A survey of the existing literature portrays the fact that the nano-composition of trihybrid nanoparticles (as in the present study) is not interpreted yet. The proposed nanoparticles such as cobalt, gold, and zirconium oxide have special characteristics owing to their thermo-physical properties. Paraffin (Pfin) which is the base fluid, in the present case, often exists in both solid and liquid form, and involves a wide range of industrial and commercial applications like beauty products, heating oil, medicines, and candles. The aim of this study is to explore the new feature of Pfin-based ternary hybrid nanofluids Co–Au–ZrO_2/Pfin incorporating the cobalt, gold, and zirconium oxide particles. The analysis is further extended to investigate the pure and hybrid case of nanofluids using Co/Pfin nanofluid and Co–Au/Pfin hybrid nanofluid.

2 Mathematical and physical aspects of the problem

A trihybrid nano-composition of zirconium oxide, cobalt, and gold nanoparticles is amalgamated in a host fluid to prepare the ternary hybrid nanofluids Co–Au–ZrO_2–Pfin. The liquid form of Pfin, in the present case, is assumed to be the base fluid. Three cases of nanofluids such as:

i) Pure nanofluid which comprises of Cobalt–Pfin,

ii) Hybrid nanofluid which comprises of Cobalt–Gold –Pfin, and

iii) Trihybrid nanofluid which comprises of Cobalt–Gold –Zirconium oxide–Pfin

are incorporated to analyze their thermal performance. The y-axis and x-axis are, respectively, taken across and along the flow over a surface. The force B_0 is applied in the same direction for which the y-axis is taken (Figure 1).

Flow is occurring through a porous medium. The velocity $U_w(x)$ represents the rate at which the surface is being stretched. The vector form of the general nanofluid flow model involving heat and mass transfer characteristics is given below:

$$\left.\begin{aligned} \rho\left(\frac{\partial \bar{u}}{\partial t} + (\bar{u}\cdot\nabla)\bar{u}\right) &= -\nabla p + \mu\nabla^2\bar{u} + \rho g,\\ \rho C_p\left(\frac{\partial T}{\partial t} + (\bar{u}\cdot\nabla)T\right) &= \nabla\cdot(k\nabla T) + \varphi,\\ \rho\left(\frac{\partial C}{\partial t} + (\bar{u}\cdot\nabla)C\right) &= \nabla\cdot(D\nabla C), \end{aligned}\right\} \quad (1)$$

where $\bar{u}$ is the velocity vector field of the fluid, ρ is the fluid density, T is the temperature, C_p is the specific heat capacity at constant pressure, φ represents any volumetric heat sources, t is the time, D is the mass diffusivity, μ is the dynamic viscosity of the fluid, $\bar{g}$ is the gravitational acceleration vector, k is the thermal conductivity, p is the pressure, and C is the concentration of the species.

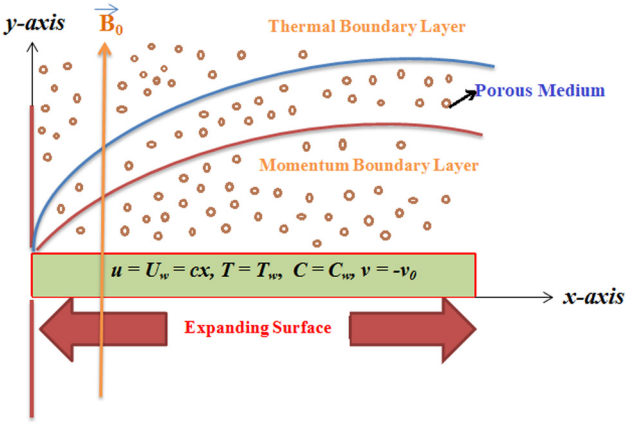

Figure 1: The problem structure.

The governing equations are followed by the recently established models [51–53] that describe the hybrid and trihybrid cases of nanofluids.

2.1 Momentum equation

The momentum equation of the problem can be given as

$$u\frac{\partial u}{\partial x} + v\frac{\partial u}{\partial y} = \upsilon_{\mathrm{Tnf}}\frac{\partial^2 u}{\partial y^2} - \frac{\mu_{\mathrm{Tnf}}}{\rho_{\mathrm{Tnf}}k^*}u - \frac{\sigma_{\mathrm{Tnf}}}{\rho_{\mathrm{Tnf}}}B_0^2 u, \quad (2)$$

Equation (2) is the derived or modified form of the Navier–Stokes momentum equation which is interlinked with the Darcy's law. This law basically governs the fluid's movement through any porous material or media. The inter-connectivity of pores in a medium is recognized as permeability. The second last term in the above equation illustrates the Darcy's law whereas the last term designates the applied magnetic field effect. The terms on the left-hand side of equation (2) represent the inertia forces. The basic task of these forces is to keep particles away from the layer. On the other hand, the first term $\upsilon_{\mathrm{Tnf}}\frac{\partial^2 u}{\partial y^2}$ on the right side of the same equation represents the viscous force that causes the smooth movement of the layers over one another. The terms in equation (2) can be communicated as follows:

ρ_{Tnf}	expresses the trihybrid nanofluid's density
u	symbolizes the horizontal velocity component
μ_{Tnf}	shows the viscosity of the trihybrid nanofluid
B_0	defines the magnetic field strength
k^*	demonstrates the permeability of the porous medium
v	signifies the vertical component of velocity
σ_{Tnf}	expresses the electrical conductivity of the trihybrid nanofluid
ν_{Tnf}	describes the trihybrid nanofluid's kinematic viscosity

2.2 Energy equation

The thermal radiation effect is assumed in the energy equation that is given below:

$$u\frac{\partial T}{\partial x} + v\frac{\partial T}{\partial y} = \frac{K_{\mathrm{Tnf}}}{(\rho C_{\mathrm{p}})_{\mathrm{Tnf}}}\frac{\partial^2 T}{\partial y^2} - \frac{1}{(\rho C_{\mathrm{p}})_{\mathrm{Tnf}}}\frac{\partial Q_{\mathrm{R}}}{\partial y}, \quad (3)$$

where the trihybrid nanofluid's thermal diffusivity is denoted by α_{hnf}, and the temperature of the fluid is represented by T. The first derivative terms like $\frac{\partial T}{\partial x}$ and $\frac{\partial T}{\partial y}$ of equation (3) describe the thermal convection whereas the term $\frac{\partial^2 T}{\partial y^2}$ portrays the thermal diffusion. The diffusion occurs because of the differences in the surface temperature and the fluid's temperature. The terms $(\rho C_{\mathrm{p}})_{\mathrm{Tnf}}$ and K_{Tnf} are used, respectively, for the heat capacity and thermal conductivity.

The term Q_{R} expresses the radiation heat flux which is often known as thermal radiation (in the dynamical problems). On the other side, thermal radiation is followed by the Rosseland's approximation (Sheikholeslami *et al.* [54,55]). By incorporating this approximation to simplify Q_{R}, we have

$$q_{\mathrm{r}} = -\frac{4\sigma}{3k_0}\frac{\partial T^4}{\partial y}, \quad (4)$$

where the mean absorption coefficient as well as the Stefan–Boltzmann constant is, respectively, represented by k_0 and σ. In order to linearize T^4 given in equation (4), we use the following relation:

$$T^4 = 4T_\infty^3 T - 3T_\infty^4, \quad (5)$$

Using relations (3) and (4), equation (3) attains the form

$$u\frac{\partial T}{\partial x} + v\frac{\partial T}{\partial y} = \frac{K_{\mathrm{Tnf}}}{(\rho C_{\mathrm{p}})_{\mathrm{Tnf}}}\frac{\partial^2 T}{\partial y^2} + \frac{16\sigma_0 T_\infty^3}{3k_0(\rho C_{\mathrm{p}})_{\mathrm{Tnf}}}\frac{\partial^2 T}{\partial y^2}, \quad (6)$$

2.3 Concentration equation

The species that are assumed to be chemically reactive are also involved in the mixture of Pfin-based trihybrid nanofluids. Due to the involvement of species, the flow will definitely contain the mass transfer phenomenon. The concentration C having unit mol/m^3, in this way, comprises of the homogeneous mixture. However, an irreversible and homogeneous reaction occurs in the flow because of the species involvement. Using these premises, the concentration equation is given by

$$u\frac{\partial C}{\partial x} + v\frac{\partial C}{\partial y} = D_{\mathrm{B}}\frac{\partial^2 C}{\partial y^2} - K_{\mathrm{r}}(C - C_\infty), \quad (7)$$

where D_{B} and K_{r} depict the mass diffusivity and chemical reaction rate constant. The term K_{r} basically determines the rate at which the chemical reaction occurs. It can be concluded from the last term (with negative sign) in the above equation that the chemical reaction tends to deteriorate the species in the flow.

2.4 Boundary conditions

The proposed boundary constraints at $y = 0$ and $y \to \infty$ have the form [56]

$$\left.\begin{aligned} &T(x,0) = T_w, \quad v(x,0) = -v_0, \\ &u(x,0) = U_w(x) = cx, \quad C(x,0) = C_w \quad \text{at } y = 0 \\ &T(x,\infty) = T_\infty, \quad u(x,\infty) = 0, \\ &C(x,\infty) = C_\infty \quad \text{at } y \to \infty \end{aligned}\right\}, \tag{8}$$

whereas the suction having velocity v_0 occurs at $v_0 > 0$. The temperatures T_∞ and T_w are specified at $y \to \infty$ and $y = 0$, respectively. In the same manners, C_w and C_∞ are the concentrations at the surface and apart from the surface. The velocity for which the surface stretches is $U(x,0) = U_w(x) = cx$.

2.5 Thermo-physical characteristics of pure, hybrid, and trihybrid nanofluids

The combination of Co, Ag, and ZrO_2 nanoparticles is taken with 0.1 volume fraction each. The ternary nanofluid (Co–Au–ZrO_2–Pfin) is prepared by the addition of Co (ϕ_1), Ag (ϕ_2), and ZrO_2 (ϕ_3) nanoparticles in the host liquid which is Pfin in the present case. The basic physical properties of the nanofluids in pure, hybrid, and trihybrid cases (engaged from the standard literature [57,58]) are portrayed in Tables 2 and 3.

The subscripts in the above Tables like Tnf, hnf, nf, f, s_1, s_2, and s_3 illustrate the ternary nanofluid, hybrid nanofluid, pure nanofluid, base fluid, solid nanoparticles of cobalt, gold, and zirconium oxide, respectively. Heat capacity in ternary case of nanofluids can be given as

$$\begin{aligned}(\rho C_p)_{Thf} = (1-\phi_3)\{(1-\phi_2)[(1-\phi_1)(\rho C_p)_f + \phi_1(\rho C_p)_{s_1}] \\ + \phi_2(\rho C_p)_{s_2}\} + \phi_3(\rho C_p)_{s_3}.\end{aligned} \tag{9}$$

2.6 Non-dimensional variables and equations

Following non-dimensional variables have been taken into consideration to change the governing equations into ordinary ones [59]:

$$\begin{aligned} &u = cxf'(\xi), \quad \xi = \sqrt{\frac{c}{\upsilon_f}}y, \quad y = \sqrt{c\upsilon_f}\, f(\xi), \\ &\theta(\xi) = \frac{T - T_\infty}{T_w - T_\infty}, \quad \phi(\xi) = \frac{C - C_\infty}{C_w - C_\infty}. \end{aligned} \tag{10}$$

Table 2: Mathematical relations for electrical and thermal conductivities of nanofluids

Nanofluids	Electrical conductivity	Thermal conductivity
Pure nanofluid	$\frac{\sigma_{nf}}{\sigma_f} = 1 + \frac{3(\sigma-1)\phi}{(\sigma+2)-(\sigma-1)\phi}$, where $\sigma = \frac{\sigma_s}{\sigma_f}$	$\frac{k_{nf}}{k_f} = \frac{k_s+(n-1)k_f-\phi(k_f-k_s)}{k_s+(n-1)k_f+\phi(k_f-k_s)}$
Hybrid nanofluid	$\frac{\sigma_{hnf}}{\sigma_{bf}} = \frac{\sigma_{s_2}+2\sigma_{bf}-2\phi_2(\sigma_{bf}-\sigma_{s_2})}{\sigma_{s_2}+2\sigma_{bf}+\phi_2(\sigma_{bf}-\sigma_{s_2})}$, where $\frac{\sigma_{bf}}{\sigma_f} = \frac{\sigma_{s_1}+2\sigma_f-2\phi_2(\sigma_f-\sigma_{s_1})}{\sigma_{s_1}+2\sigma_f+\phi_2(\sigma_f-\sigma_{s_1})}$	$\frac{k_{hnf}}{k_{bf}} = \frac{k_{s_2}+(n-1)k_{bf}-\phi_2(n-1)(k_{bf}-k_{s_2})}{k_{s_2}+(n-1)k_{bf}+\phi_2(k_{bf}-k_{s_2})}$, where $\frac{k_{bf}}{k_f} = \frac{k_{s_1}+(n-1)k_f-\phi_1(k_f-k_{s_1})}{k_{s_1}+(n-1)k_f+\phi_1(k_f-k_{s_1})}$
Trihybrid nanofluid	$\frac{\sigma_{Tnf}}{\sigma_{hnf}} = \frac{(1+2\phi_3)\sigma_{s_3}+(1-2\phi_3)\sigma_{hnf}}{(1-\phi_3)\sigma_{s_3}+(1+\phi_3)\sigma_{hnf}}$ $\frac{\sigma_{hnf}}{\sigma_{nf}} = \frac{(1+2\phi_2)\sigma_{s_2}+(1-2\phi_2)\sigma_{nf}}{(1-\phi_2)\sigma_{s_2}+(1+\phi_2)\sigma_{nf}}$, $\frac{\sigma_{nf}}{\sigma_f} = \frac{(1+2\phi_1)\sigma_{s_1}+(1-2\phi_1)\sigma_f}{(1-\phi_1)\sigma_{s_1}+(1+\phi_1)\sigma_f}$,	$\frac{k_{Tnf}}{k_{hnf}} = \frac{k_{s_3}+2k_{hnf}-2\phi_3(k_{hnf}-k_{s_3})}{k_{s_3}+2k_{hnf}+\phi_3(k_{hnf}-k_{s_3})}$, $\frac{k_{hnf}}{k_{nf}} = \frac{k_{s_2}+2k_{nf}-2\phi_2(k_{nf}-k_{s_2})}{k_{s_2}+2k_{nf}+\phi_2(k_{nf}-k_{s_2})}$, $\frac{k_{nf}}{k_f} = \frac{k_{s_1}+2k_f-2\phi_1(k_f-k_{s_1})}{k_{s1}+2k_f+\phi_1(k_f-k_{s_1})}$,

Table 3: Mathematical relations for viscosity and density of nanofluids

Nanofluids	Viscosity	Density
Pure nanofluid	$\mu_{nf} = \frac{\mu_f}{(1-\phi)^{2.5}}$	$\rho_{nf} = (1-\phi)\rho_f + \phi\rho_s$
Hybrid nanofluid	$\mu_{hnf} = \frac{\mu_f}{(1-\phi_1)^{2.5}(1-\phi_2)^{2.5}}$	$\rho_{hnf} = \{(1-\phi_2)[(1-\phi_1)\rho_f + \phi_1\rho_{s_1}]\} + \phi_2\rho_{s_2}$
Trihybrid nanofluid	$\mu_{Tnf} = \frac{\mu_f}{(1-\phi_1)^{2.5}(1-\phi_2)^{2.5}(1-\phi_3)^{2.5}}$	$\rho_{Thf} = (1-\phi_3)\left\{\begin{matrix}(1-\phi_2)[(1-\phi_1)\rho_f + \phi_1\rho_{s_1}]+ \\ \phi_2\rho_{s_2}\end{matrix}\right\} + \phi_3\rho_{s_3}$

Employing the above relations in equations (2)–(4), we get

$$f''' = \Delta_0 + \Delta_1(f'^2 - ff'') + P_0 f' + \Delta_2 M_0 f', \tag{11}$$

$$\frac{1}{\Pr}\left(\frac{K_{\text{Tnf}}}{K_{\text{f}}} + \frac{4}{3}R_{\text{d}}\right)\theta'' + \Delta_4 f\theta' = 0, \tag{12}$$

$$\frac{1}{\text{Sc}}\phi'' + f\phi' - K_{\text{c}}\phi = 0, \tag{13}$$

where

$$\Delta_0 = (1-\phi_3)(1-\phi_2)(1+2\phi_3)\sigma_{s_3} + (1-2\phi_3)\sigma_{s_f} + \phi_2(1 - \phi_3)\sigma_{s_3} + (1+\phi_3)\sigma_{\text{f}} + \phi_3\left(\frac{\rho_{s_3}}{\rho_{\text{f}}}\right)^{-1}, \tag{14}$$

$$\Delta_1 = (1-\phi_1)^{2.5}(1-\phi_2)^{2.5}(1-\phi_3)^{2.5}\Bigg[(1 - \phi_2)\left\{(1-\phi_1) + \phi_1\frac{\rho_{s_1}}{\rho_{\text{f}}}\right\} + \phi_2\frac{\rho_{s_2}}{\rho_{\text{f}}}\Bigg] + \phi_3\frac{\rho_{s_3}}{\rho_{\text{f}}}, \tag{15}$$

$$\Delta_2 = (1-\phi_1)^{2.5}(1-\phi_2)^{2.5}(1-\phi_3)^{2.5}\frac{\sigma_{\text{Tnf}}}{\sigma_{\text{f}}}, \tag{16}$$

$$\Delta_3 = \frac{K_{\text{Tnf}}}{K_{\text{f}}} + \frac{4}{3}R_{\text{d}}, \tag{17}$$

$$\Delta_4 = \Bigg[(1-\phi_2)(1-\phi_3)\left\{(1-\phi_1) + \phi_1\frac{(\rho c_{\text{p}})_{s_1}}{(\rho c_{\text{p}})_{\text{f}}}\right\} + \phi_2\frac{(\rho c_{\text{p}})_{s_2}}{(\rho c_{\text{p}})_{\text{f}}}\Bigg] + \phi_3\frac{(\rho c_{\text{p}})_{s_3}}{(\rho c_{\text{p}})_{\text{f}}}, \tag{18}$$

Boundary conditions (5), in the light of (6), take new form as follows:

$$\left.\begin{aligned}&\xi = 0 \quad f = S, \quad f' = 1, \quad \theta = 1, \quad \phi = 1,\\ &\xi \to \infty \quad f' \to 0, \quad \theta \to 0, \quad \phi \to 0.\end{aligned}\right\} \tag{19}$$

where $S_{\text{uc}} = \frac{v_0}{\sqrt{cv_{\text{f}}}}$ denotes the suction phenomenon.

2.7 Problem parameters

The preeminent parameters can be specified as follows:

ϕ_1	is the nanoparticles volume concentration of cobalt
$M_0^2 = \frac{\sigma_{\text{f}}B_0^2}{c\rho_{\text{f}}}$	is the magnetic interaction parameter
$Ch_{\text{R}} = \frac{K_{\text{r}}x}{U_{\text{w}}}$	is the chemical reaction parameter
$\text{Por} = \frac{v_{\text{f}}}{ck^*}$	is the porosity parameter
ϕ_2	is the nanoparticles volume concentration of gold
$\Pr = \frac{\mu_{\text{f}}(c_{\text{p}})_{\text{f}}}{k_{\text{f}}}$	is the Prandtl number
$T_{\text{Rad}} = \frac{4\sigma_0 T_\infty^3}{k_0 k_{\text{f}}}$	is the thermal radiation parameter
$\text{Sc}_0 = \frac{v_{\text{f}}}{D_{\text{B}}}$	is the Schmidt number
ϕ_1	is the nanoparticles volume concentration of zirconium oxide

The prime quantities of the engineering applications may be described as

$$\begin{aligned}&\text{Re}_x^{\frac{1}{2}}C_{\text{f}x} = \frac{f''(0)}{(1-\phi_1)^{2.5}(1-\phi_2)^{2.5}(1-\phi_3)^{2.5}},\\ &\text{Nu}_x\,\text{Re}_x^{\frac{1}{2}} = -\frac{k_{\text{Tnf}}}{k_{\text{f}}}\theta'(0), \quad \text{Sh}_x\,\text{Re}_x^{\frac{1}{2}} = -\phi'(0).\end{aligned} \tag{20}$$

The Reynolds number in the above equation is described by the relation $\text{Re}_x = \frac{U_{\text{w}}x}{v_{\text{f}}}$. The properties of the base fluid as well as three different nanoparticles are specified in Table 4.

The local thermo-fluid flow behavior (in terms of streamline and isotherms) is portrayed in Figures 2 and 3.

Table 4: Thermal properties of Pfin, cobalt, gold, and zirconium oxide

Properties	Paraffin (Pfin) (f)	Cobalt (Co) (s_1)	Gold (Au) (s_2)	Zirconium oxide (ZrO_2) (s_3)
σ(s/m)	1.6×10^{-14}	1.602×10^7	4.5×10^7	2.4×10^{-6}
k(W/mK)	0.23	100	320	1.7
ρ(kg/m^3)	802	8,900	19,300	5,680
C_{p}(J/kg K)	2,320	420	129.1	502

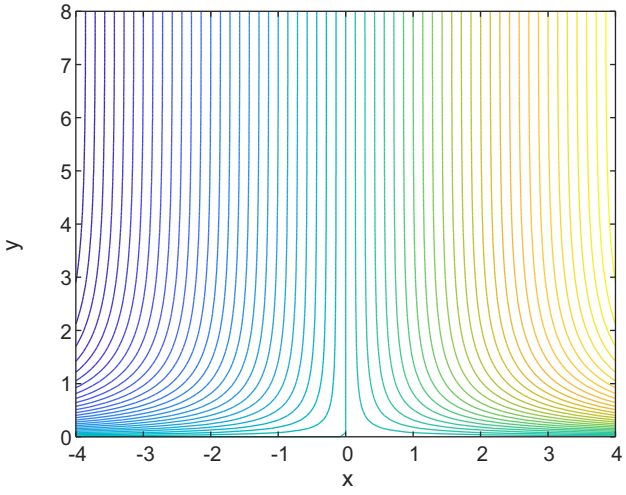

Figure 2: Streamlines for the flow when Pr = 6.2, Sc = 1.5, and M = 5.

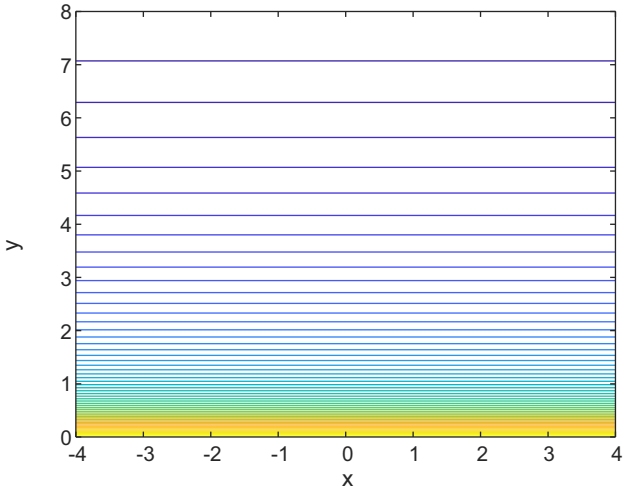

Figure 3: Isotherm for the temperature distribution when Pr = 6.2, Sc = 1.5, and M = 5.

3 Solution methodology

The analytical solution of equations (11)–(13) might be so much complicated as these equations are not only coupled but also highly nonlinear. A suitable numerical technique may be the better choice to find the approximate solutions of the problem. However, Successive over Relaxation Method which is based on Gauss–Seidel iteration method is incorporated for the purpose of simulation analysis. This technique involves a relaxation factor for which the required convergence can be attained. This factor accelerates the convergence, and takes the value which is (in general) less than 1. The smaller steps or step sizes, in this method,

Table 5: A heat transfer rate comparison when Prandtl number changes and $\phi_1 = \phi_2 = \phi_3 = 0$

Pr	Devi and Devi [60]	Ahmad *et al.* [61]	Khan and Pop [62]	Present results
2	0.91135	0.91045	0.9113	0.91045
7	1.89540	1.89083	1.8954	1.89083
20	3.35390	3.35271	3.3539	3.35271

leads toward the final solution. To initiate the iterative procedure, we set the equations (11)–(13) as follows:

$$\left.\begin{aligned} f(i) &= (W/A_0)*(A_1*p(i+1) + A_2*p(i-1) + A_3) \\ &\quad + (1-W)*f(i), \\ \theta(i) &= (W/B_0)*(B_1*\theta(i+1) + B_2*\theta(i-1) + B_3) \\ &\quad + (1-W)*\theta(i), \\ \phi(i) &= (W/C_0)*(C_1*\phi(i+1) + C_2*\phi(i-1) + C_3) \\ &\quad + (1-W)*\phi(i). \end{aligned}\right\} \quad (21)$$

where W is the relaxation factor such that $W < 1$. Table 5 provides a comparison which validates the results and assures the accuracy of the numerical procedure. The main steps of the adopted methodology are mentioned in the flow chart diagram (Figure 4). The numerical uncertainty analysis is presented in Table 6. Numerical values of $f(\eta)$ corresponding to the step size h can be analyzed from this table.

4 Results and discussion

In this section, the numerical consequences of the preeminent parameters are discussed by the physical interpretations of the graphs and tables. The flow and thermal characteristics of the pure nanofluid Co−Pfin, hybrid nanofluid Co−Au−Pfin, and trihybrid nanofluid Co−Au−ZrO_2−Pfin are elaborated in this study. An asymptotic behavior (in graphical profiles) is achieved by appropriately choosing the step sizes. Assigning the suitable dimensionless values to the parameters might provide better consequences in factual employments of the work rather than proposing the fluid characteristics and particular domains [63,64]. According to these lines, the simulation process is carried out using $T_{\mathrm{Rad}} = 0.2$, $\mathrm{Sc}_0 = 1.5$, $M_0 = 2$, $\mathrm{Ch}_{\mathrm{R}} = 4$, Por = 2, Pr = 6.135, and $\phi_1 = \phi_2 = \phi_3 = 0.1$ unless otherwise apportioned.

Figures 5 and 6 are depicted to elucidate the velocity $F'(\eta)$ and temperature $\theta(\eta)$ for three cases of nanofluids with change in magnetic interaction parameter M_0. The first case indicates the pure nanofluids Co–Pfin

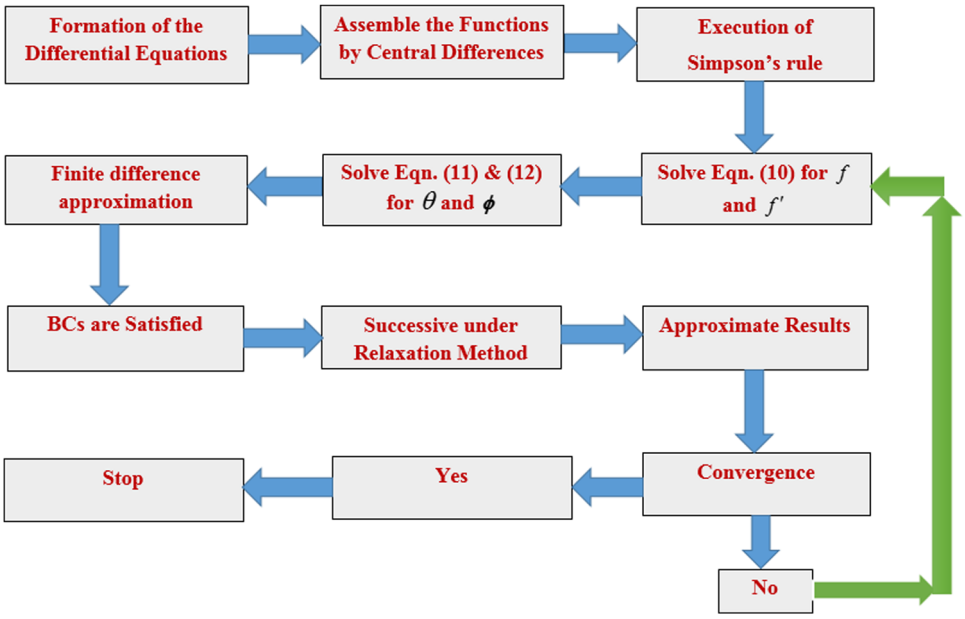

Figure 4: Flow chart diagram for numerical scheme.

Table 6: Numerical values of $f(\eta)$ corresponding to the step size h

η	$f(\eta)$			Change in error in $f(\eta)$	
	$h = 0.05$	$\frac{h}{2} = 0.025$	$\frac{h}{4} = 0.0125$	From h to $\frac{h}{2}$	From $\frac{h}{2}$ to $\frac{h}{4}$
0.5	0.34974940	0.34889300	0.34867867	0.000856788	2.1433085×10^{-4}
1.0	0.43469733	0.43345392	0.43314171	0.001243410	3.1220685×10^{-4}
1.5	0.46581887	0.46441823	0.46406630	0.001400644	3.5192816×10^{-4}
2.0	0.47945838	0.47798565	0.47761552	0.001472729	3.7012717×10^{-4}
2.5	0.48610751	0.48459873	0.48421951	0.001508775	3.7922471×10^{-4}
3.0	0.48958050	0.48805259	0.48766854	0.001527911	3.8405277×10^{-4}
3.5	0.49146811	0.48992968	0.48954298	0.001538424	3.8670473×10^{-4}
4.0	0.49249417	0.49094998	0.49056183	0.001544180	3.8815634×10^{-4}
4.5	0.49300307	0.49145602	0.49106714	0.001547047	3.8887926×10^{-4}
5.0	0.49315526	0.49160735	0.49121825	0.001547906	3.8909581×10^{-4}

($\phi_1 = 0.1$ and $\phi_2 = \phi_3 = 0.1$), the second one represents the hybrid nanofluid Co–Au–Pfin ($\phi_1 = \phi_2 = 0.1$ and $\phi_3 = 0$), and the third one is for the ternary case of nanofluids Co–Au–ZrO_2–Pfin ($\phi_1 = \phi_2 = \phi_3 = 0.1$). The velocity is decreased and the temperature is increased by the magnetic field. The applied magnetic field is one of the factors which originates the Lorentz force. When the magnetic and electric field interact during the motion of an electrically conducting fluid, then it gives rise to the Lorentz force. The retarding force, in the present case, increases when the levels (values) of magnetic field parameter are increased. Subsequently, the fluid velocity decreases and the temperature of fluid increases with the magnetic field.

The dimensionless velocity as well as temperature profile is appeared in Figures 7 and 8. In either case of nanofluids, velocity is reduced by the porosity of the medium but the temperature of fluid tends to increase with this parameter. A declination in the velocity is associated with the pores size within the permeable media. In this case, fluid faces resistance when it passes through the pores. An important fact noted is that the smaller values of porosity parameter interrupt the solution. This fact may be attributed because of the involvement of three distinct types of nanoparticles which require large pore size to pass through them. However, we assigned large values to the porosity parameter unless otherwise optimal state of solution does not achieve.

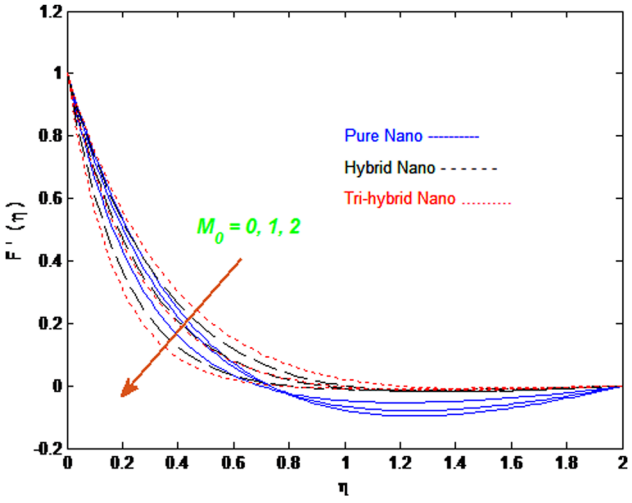

Figure 5: Velocity $F'(\eta)$ for three cases of nanofluids with change in M_0.

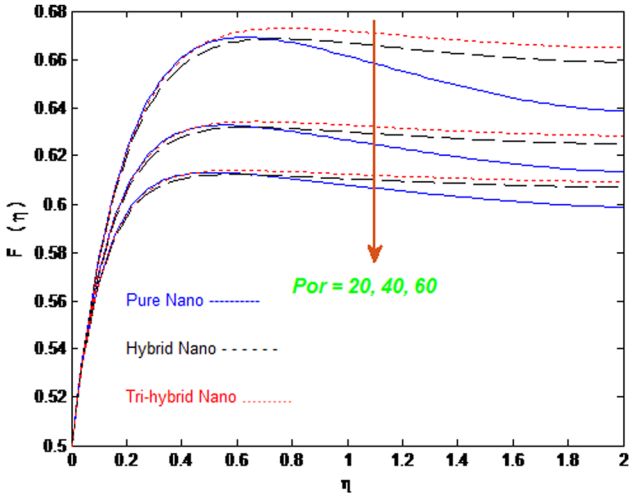

Figure 7: Velocity $F(\eta)$ for three cases of nanofluids with change in Por.

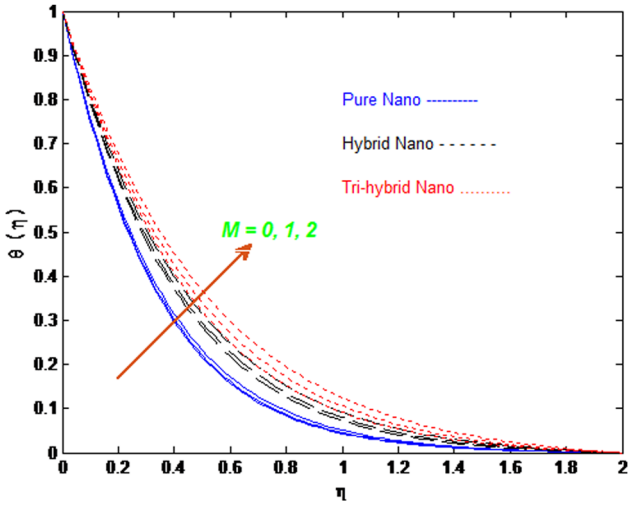

Figure 6: Temperature $\theta(\eta)$ for three cases of nanofluids with change in M_0.

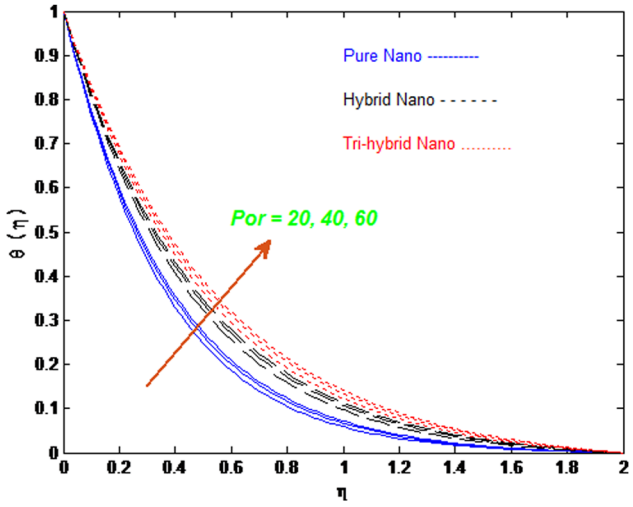

Figure 8: Temperature $\theta(\eta)$ for three cases of nanofluids with change in Por.

It is noted from Tables 7 and 8 that the porosity parameter has dominant effect on the skin friction as compared to the magnetic parameter. Both these parameters tend to upsurge the shear stress but deteriorate the heat transfer rate in either case of nanofluids (usual, hybrid, and ternary nanofluid). It is better to mention that material porosity has higher influence on the skin friction as compared to the magnetic field parameter. On the other hand, both these parameters insert low effect on the Nusselt number.

The consequences of Figure 9 articulate that the temperature decreases with an increase in the dimensionless values of Prandtl number. It may have happened due to the

Table 7: Skin frictions for three cases of nanofluids with change in Por and M_0

Parameters		Skin frictions		
Por	M_0	Pure nano	Hybrid nano	Trihybrid nano
20		−6.8745974	−9.4005197	−11.9779623
40		−9.0386709	−12.1977051	−15.6280456
60		−10.7246677	−14.3779038	−18.4707024
	0	−3.9669009	−5.3127986	−6.2827091
	1	−4.2398968	−6.2006625	−8.3972919
	2	−5.2138095	−8.3124442	−12.6196198

Table 8: Nusselt numbers for three cases of nanofluids with change in Por and M_0

Parameters		Nusselt numbers		
Por	M_0	**Pure nano**	**Hybrid nano**	**Trihybrid nano**
20		3.4789813	3.7523867	4.0469349
40		3.3750103	3.6295708	3.9041364
60		3.3118644	3.5568421	3.8212620
	0	3.6586039	4.0123214	4.4044729
	1	3.6336487	3.9515072	4.2484228
	2	3.5794819	3.8121882	4.01805868

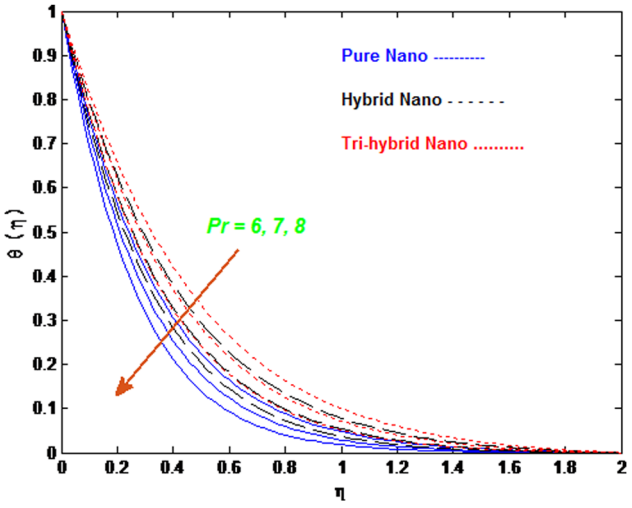

Figure 9: Temperature $\theta(\eta)$ for three cases of nanofluids with change in Pr.

relatively high thermal diffusivity of fluid as equated to kinematic viscosity. Variation in the temperature $\theta(\eta)$ for three (usual, hybrid, and ternary) cases of nanofluids with change in thermal radiation T_{Rad}, volume fraction ϕ_2 of gold, and volume fraction ϕ_3 of zirconium oxide is portrayed in Figures 10–12. The temperature profiles seem to be increasing with these three parameters in all cases of nanofluids. Out of three heat transfer modes, thermal radiation is one of them whereas the other two are convection and conduction. When the thermal radiation emitted from the source is absorbed by the fluid, then it would definitely elevate the temperature. The trihybrid nano case is more prominent in order to enhance the temperature throughout the flow regime. The amalgamation of three distinct nanoparticles in base fluid exhibits improved overall thermal characteristics as related to the single or binary components nanofluids. This is the reason that we have noticed high temperature in ternary nanofluid case other than the mono or hybrid case.

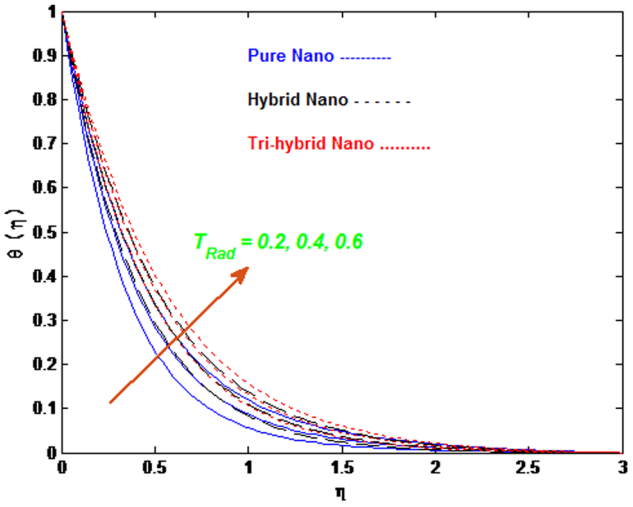

Figure 10: Temperature $\theta(\eta)$ for three cases of nanofluids with change in T_{Rad}.

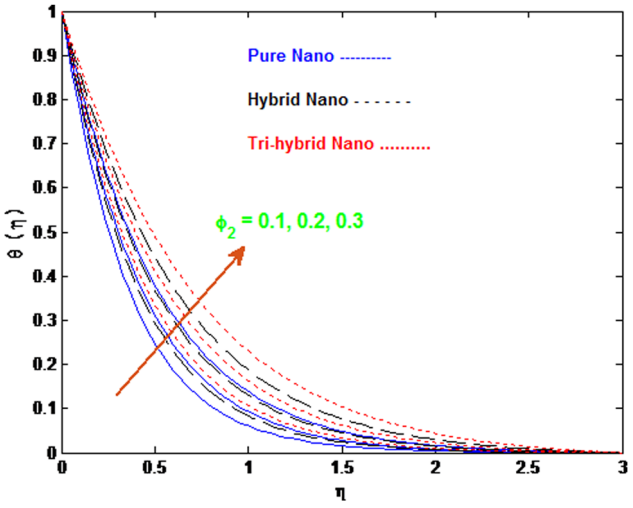

Figure 11: Temperature $\theta(\eta)$ for three cases of nanofluids with change in ϕ_2.

Heat transfer rate is increased by the volume fraction of gold (Au), Prandtl number (Pr), and volume fraction of zirconium oxide (ZrO_2) (Table 9). However, a decrease in the Nusselt number is observed when the thermal radiation parameter T_{Rad} is increased. It is noticeable that trihybrid nanofluids (Co–Au–ZrO_2–Pfin) have marginally increased heat transmission rate as compared to the other two cases. If we comparatively analyze the impact of ϕ_2 and ϕ_3, which are, respectively, nanoparticles volume fractions of gold and zirconium oxide on the Nusselt number, then we conclude that the volume fraction of ZrO_2 has a significant impact on Nu.

Figures 13 and 14 portray the concentration profiles $\phi(\eta)$ against the parameter of chemical reaction Ch_R and

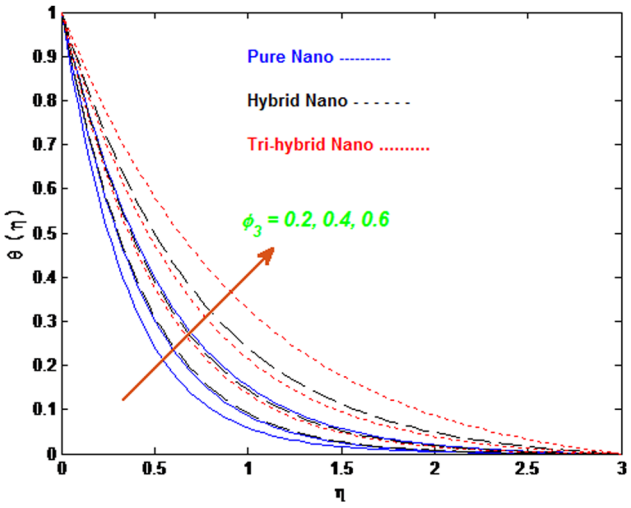

Figure 12: Temperature $\theta(\eta)$ for three cases of nanofluids with change in ϕ_3.

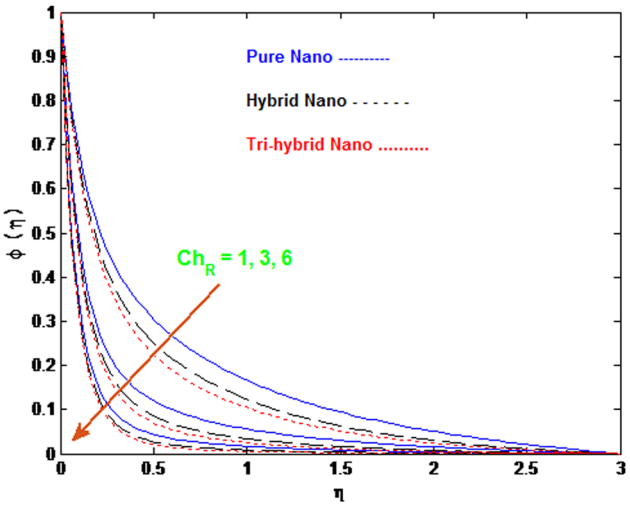

Figure 13: Concentration $\phi(\eta)$ for three cases of nanofluids with change in Ch_R.

Table 9: Nusselt numbers for three cases of nanofluids with change in Pr, T_{Rad}, ϕ_2, and ϕ_3

Parameters				Nusselt numbers		
Pr	T_{Rad}	ϕ_2	ϕ_3	Pure nano	Hybrid nano	Trihybrid nano
6				3.5503990	3.9176022	4.2716610
7				4.1056182	4.5105642	4.9120449
8				4.6482035	5.0936047	5.5424835
	0.2			3.6261513	3.9982474	4.3586809
	0.4			3.1291554	3.5723390	3.9657133
	0.6			2.7500112	3.2314996	3.6414327
		0.1		3.4390635	3.9982474	4.3586809
		0.2		3.7764852	4.3068073	4.6556849
		0.3		4.1151896	4.6151008	4.9393795

the Schmidt number Sc_0. Both the profiles are noticed to be decelerating with the prominent effects of Ch_R and the Schmidt number Sc_0. This fact may be attributed to the reason that the mass diffusivity is reduced by the Schmidt number as well as chemical reaction parameter. Hence, concentration is decreased in the flow regime. One of the other reasons is the viscous diffusion which increases when Sc_0 increases and, consequently, concentration is declined. It can be revealed from Table 10 that the mass transfer rate is significantly increased in all (pure, hybrid, and trihybrid) cases of nanofluids with the effects of chemical reaction parameter and Schmidt number. Effects of different prime parameters on the flow dynamics can be studied from previous literature [65–76].

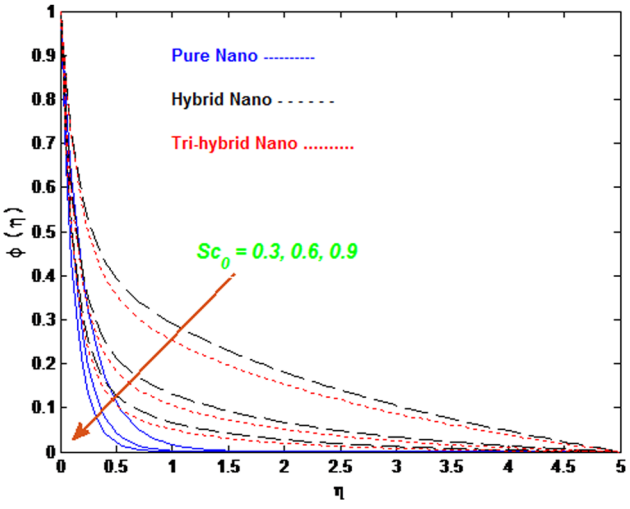

Figure 14: Concentration $\phi(\eta)$ for three cases of nanofluids with change in Sc_0.

Table 10: Sherwood numbers for three cases of nanofluids with change in Ch_R and Sc_0

Parameters		Sherwood numbers		
Ch_R	Sc_0	Pure nano	Hybrid nano	Trihybrid nano
1		4.4429811	4.7350108	4.8865235
3		8.3545029	8.6694166	8.8258259
6		12.0034633	12.3101431	12.4624268
	0.3	3.4616350	3.7456153	3.8991065
	0.6	5.5712367	5.8910443	6.0536072
	0.9	7.2066153	7.5271109	7.6868220

5 Conclusion

The appropriate combination of nanoparticles in trihybrid nanofluids is mainly based on the specific properties and desired applications. For instance, some of the nanoparticles enhance the heat transfer characteristics and some types of nano-sized particles might deliver improved thermal conductivity. An effort is taken out to examine the change in flow and thermal features of the problem for three cases of nanofluids: (i) pure nanofluids, (ii) hybrid nanofluids, and (iii) ternary hybrid nanofluids. The nanocomposition of three distinct particles (ternary case of nanofluids) can lead toward the higher thermal conductivity, embellished heat transfer efficiency and the other required features. The current work aims to investigate the features of Pfin-based trihybrid nanofluids which consist of cobalt, gold, and zirconium oxide nanoparticles. The main consequences of the present work are enlisted below

a) The trihybrid nanofluids (Co–Au–ZrO_2–Pfin) have marginally increased the heat transfer rate as compared to the other two cases, *e.g.*, pure and hybrid nanofluid case.
b) The porosity as well as magnetic interaction parameter tends to upsurge the shear stress but deteriorate the heat transfer rate in usual, hybrid, and ternary case of nanofluids.
c) In either case of nanofluids, velocity is reduced by the porosity of the medium but the temperature of fluid tends to increase with this parameter.
d) The temperature profiles seem to be increasing with the change (increase) in thermal radiation T_{Rad}, volume fraction ϕ_2 of gold, and volume fraction ϕ_3 of zirconium oxide.
e) The velocity of fluid decreases whereas the temperature increases due to the magnetic field in all cases.
f) The volume fraction ϕ_3 of ZrO_2 has a significant impact on Nusselt number rather than ϕ_2 which is volume fraction of gold (Au).
g) The prominent effects of chemical reaction $\mathrm{Ch_R}$ and the Schmidt number $\mathrm{Sc_0}$ cause a deceleration in the concentration of hybrid and ternary hybrid nanofluids.

Acknowledgments: The authors extend their appreciation to the Deanship of Scientific Research at King Khalid University for funding this work through small group Research Project under grant number RGP.1/97/44.

Funding information: The authors extend their appreciation to the Deanship of Scientific Research at King Khalid University for funding this work through small group Research Project under grant number RGP.1/97/44.

Author contributions: D.Y. and S.A. formulated the problem. K.A. and W.J. solved the problem. D.Y., S.A., K.A., S.A., T.A., W.J., S.M.H., K.I., and H.A. computed and scrutinized the results. All authors have accepted responsibility for the entire content of this manuscript and approved its submission.

Conflict of interest: The authors state no conflict of interest.

Data availability statement: Data sharing is not applicable to this article as no datasets were generated or analyzed during the current study.

References

[1] Mandal DK, Biswas N, Manna NK, Gorla RSR, Chamkha AJ. Hybrid nanofluid magnetohydrodynamic mixed convection in a novel W-shaped porous system. Int J Numer Methods Heat Fluid Flow. 2023;33(2):510–44. doi: 10.1108/HFF-03-2022-0163.
[2] Biswas N, Mandal DK, Manna NK, Gorla RSR, Chamkha AJ. Hybridized nanofluidic convection in umbrella-shaped porous thermal systems with identical heating and cooling surfaces. Int J Numer Methods Heat Fluid Flow. 2023;33(9):3164–201. doi: 10.1108/HFF-11-2022-0639.
[3] Mondal MK, Mandal DK, Biswas N, Manna NK, Khaled A-F, Chamkha AJ. Enhanced magneto-convective heat transport in porous hybrid nanofluid systems with multi-frequency nonuniform heating. J Magn Magn Mater. 2023;577:170794. doi: 10.1016/j.jmmm.2023.170794.
[4] Yasmin H, Giwa SO, Noor S, Sharifpur M. Experimental Exploration of hybrid nanofluids as energy-efficient fluids in solar and thermal energy storage applications. Nanomaterials. 2023;13:278. doi: 10.3390/nano13020278.
[5] Yasmin H, Giwa SO, Noor S, Aybar HS. Influence of preparation characteristics on stability, properties, and performance of mono- and hybrid nanofluids: current and future perspective. Machines. 2023;11:112. doi: 10.3390/machines11010112.
[6] Gupta SK, Sharma A. A brief review of nanofluids utilization in heat transfer devices for energy saving. Mater Today: Proc. 2023. doi: 10.1016/j.matpr.2023.03.364.
[7] Tembhare SP, Barai DP, Bhanvase BA. Performance evaluation of nanofluids in solar thermal and solar photovoltaic systems: A comprehensive review. Renew Sustain Energy Rev. 2022;153:111738.
[8] Sun L, Yang L, Zhao N, Song J, Li X, Wu X. A review of multifunctional applications of nanofluids in solar energy. Powder Tech. 2022;411:117932.
[9] Panduro C, Finotti EA, F. A review of the use of nanofluids as heat-transfer fluids in parabolic-trough collectors. Appl Therm Eng. 2022;211:118346.
[10] Jakeer S, Reddy PBA, Reddy SRR, Basha HT. Entropy generation and melting heat transfer on the ferrohydrodynamic flow of Fe_3O_4-Ag/blood hybrid nanofluid with Cattaneo-Christov heat flux model. Waves Random Complex Media. 2023;1–24. doi: 10.1080/17455030.2022.2164808.

[11] Maatoug S, Abbasi A, Farooq W, Khan SU, Ghachem K, Aich W, et al. Bioconvective Homann flow of tangent hyperbolic nanofluid due to spiraling disk with convective and zero mas flux constraints. J Indian Chem Soc. 2023;100(1):100819. doi: 10.1016/j.jics.2022.100819.

[12] Rahman Salari S, Khavarpour M, Masoumi M, Mosivand S. Preparation of cobalt oxide and tin dioxide nanofluids and investigation of their thermophysical properties. Microfluid Nanofluid. 2022;26:79. doi: 10.1007/s10404-022-02585-5.

[13] Sekhar TVR, Nandan G, Prakash R, Muthuraman M. Investigations on viscosity and thermal conductivity of cobalt oxide-water nano fluid. Mater Today: Proc. 2018;5(2):6176–82. doi: 10.1016/j.matpr.2017.12.224.

[14] Farooq U, Waqas H, Fatima N, Imran M, Noreen S, Bariq A, et al. Computational framework of cobalt ferrite and silver-based hybrid nanofluid over a rotating disk and cone: A comparative study. Sci Rep. 2023;13:5369. doi: 10.1038/s41598-023-32360-7.

[15] Murtaza S, Kumam P, Bilal M, Sutthibutpong T, Rujisamphan N, Ahmad Z. Parametric simulation of hybrid nanofluid flow consisting of cobalt ferrite nanoparticles with second-order slip and variable viscosity over an extending surface. Nanotechnol Rev. 2023;12(1):20220533. doi: 10.1515/ntrev-2022-0533.

[16] Santhosh N, Sivaraj R. Comparative heat transfer performance of hydromagnetic mixed convective flow of cobalt-water and cobalt-kerosene ferro-nanofluids in a porous rectangular cavity with shape effects. Eur Phys J Plus. 2023;138:240. doi: 10.1140/epjp/s13360-023-03837-1.

[17] Mandal DK, Biswas N, Manna NK, Gorla RSR, Chamkha AJ. Role of surface undulation during mixed bioconvective nanofluid flow in porous media in presence of oxytactic bacteria and magnetic fields. Int J Mech Sci. 2021;211:106778. doi: 10.1016/j.ijmecsci.2021.106778.

[18] Biswas N, Manna NK, Mandal DK, Gorla RSR. Magnetohydrodynamic mixed bioconvection of oxytactic microorganisms in a nanofluid-saturated porous cavity heated with a bell-shaped curved bottom. Int J Numer Methods Heat Fluid Flow. 2021;31(12):3722–51. doi: 10.1108/HFF-10-2020-0668.

[19] Biswas N, Mandal DK, Manna NK, Benim AC. Magneto-hydro-thermal triple-convection in a W-shaped porous cavity containing oxytactic bacteria. Sci Rep. 2022;12:18053. doi: 10.1038/s41598-022-18401-7.

[20] Tsai CY, Chien HT, Ding PP, Chan B, Luh TY, Chen PH. Effect of structural character of gold nanoparticles in nanofluid on heat pipe thermal performance. Mater Lett. 2004;58(9):1461–5. doi: 10.1016/j.matlet.2003.10.009.

[21] Khan A, Alyami MA, Alghamdi W, Alqarni MM, Yassen MF, Tag Eldin E. Thermal examination for the micropolar gold–blood nanofluid flow through a permeable channel subject to gyrotactic microorganisms. Front Energy Res. 2022;10:993247. doi: 10.3389/fenrg.2022.993247.

[22] Magodora M, Mondal H, Motsa S, Sibanda P. Numerical studies on gold-water nanofluid flow with activation energy past a rotating disk. Int J Appl Comput Math. 2022;8:41. doi: 10.1007/s40819-022-01241-4.

[23] Srinivas S, Vijayalakshmi A, Subramanyam Reddy A. Flow and heat transfer of gold-blood nanofluid in a porous channel with moving/stationary walls. J Mech. 2017;33(3):395–404. doi: 10.1017/jmech.2016.102.

[24] Burgos J, Mondragón R, Elcioglu EB, Fabregat-Santiago F, Hernández L. Experimental characterization and statistical analysis of water-based gold nanofluids for solar applications: optical properties and photothermal conversion efficiency. RRL Sol. 2022;6(7):2200104. doi: 10.1002/solr.202200104.

[25] Alktranee M, Shehab MA, Németh Z, Bencs P, Hernadi K. Effect of zirconium oxide nanofluid on the behaviour of photovoltaic–thermal system: An experimental study. Energy Rep. 2023;9:1265–77. doi: 10.1016/j.egyr.2022.12.065.

[26] Souayeh B. Simultaneous features of cc heat flux on dusty ternary nanofluid (Graphene + Tungsten Oxide + Zirconium Oxide) through a magnetic field with slippery condition. Mathematics. 2023;11:554. doi: 10.3390/math11030554.

[27] Cheng H, Jianxun S, Cheng L, Lina W, Changchun Z, Xingdong Z. Synthesis of nano zirconium oxide and its application in dentistry. Nanotech Rev. 2019;8(1):396–404. doi: 10.1515/ntrev-2019-0035.

[28] Sun C, Fard BE, Karimipour A, Abdollahi A, Bach QV. Producing ZrO_2/LP107160 NF and presenting a correlation for prediction of thermal conductivity via GMDH method: An empirical and numerical investigation. Phys E: Low Dimens Syst Nanost. 2021;127:114511. doi: 10.1016/j.physe.2020.114511.

[29] Ali K, Ahmad S, Ahmad S, Jamshed W, Tirth V, Algahtani A, et al. Insights into the thermal attributes of sodium alginate ($NaC_6H_7O_6$) based nanofluids in a three-dimensional rotating frame: A comparative case study. Case Stud. Therm Eng. 2023;49:103211. doi: 10.1016/j.csite.2023.103211.

[30] Shao Y, Nayak MK, Dogonchi AS. Ternary hybrid nanofluid natural convection within a porous prismatic enclosure with two movable hot baffles: An approach to effective cooling. Case Stud Therm Eng. 2022;40:102507. doi: 10.1016/j.csite.2022.102507.

[31] Adun H, Kavaz D, Dagbasi M. Review of ternary hybrid nanofluid: Synthesis, stability, thermophysical properties, heat transfer applications, and environmental effects. J Clean Prod. 2021;328:129525. doi: 10.1016/j.jclepro.2021.129525.

[32] Algehyne EA, Alrihieli HF, Bilal M. Numerical approach toward ternary hybrid nanofluid flow using variable diffusion and non-Fourier's concept. ACS Omega. 2022;7(33):29380–90.

[33] Elnaqeeb T, Animasaun IL, Shah NA. Ternary-hybrid nanofluids: significance of suction and dual-stretching on three-dimensional flow of water conveying nanoparticles with various shapes and densities. Z Naturforschung A. 2021;76(3):231–43. doi: 10.1515/zna-2020-0317.

[34] Li S, Puneeth V, Saeed AM, Singhal A, Al-Yarimi F, Khan MI, et al. Analysis of the Thomson and Troian velocity slip for the flow of ternary nanofluid past a stretching sheet. Sci Rep. 2023;13:2340. doi: 10.1038/s41598-023-29485-0.

[35] Yasmin H, Giwa SO, Noor S, Aybar HS. Reproduction of nanofluid synthesis, thermal properties and experiments in engineering: a research paradigm shift. Energies. 2023;16:1145. doi: 10.3390/en16031145.

[36] Yasmin H, Giwa SO, Noor S, Sharifpur M. Thermal conductivity enhancement of metal oxide nanofluids: a critical review. Nanomaterials. 2023;13:597. doi: 10.3390/nano13030597.

[37] Jan A, Mushtaq M, Farooq U, Hussain M. Nonsimilar analysis of magnetized Sisko nanofluid flow subjected to heat generation/absorption and viscous dissipation. J Magn Magn Mater. 2022;564:170153. doi: 10.1016/j.jmmm.2022.170153.

[38] Farooq J, Chung JD, Mushtaq M, Lu D, Ramazan M, Farooq U. Influence of slip velocity on the flow of viscous fluid through a porous medium in a permeable tube with a variable bulk flow rate. Results Phys. 2018;11:861–8. doi: 10.1016/j.rinp.2018.10.049.

[39] Riaz S, Afzaal MF, Wang Z, Jan A, Farooq U. Numerical heat transfer of non-similar ternary hybrid nanofluid flow over linearly

stretching surface. Numer Heat Transf, Part A: Appl. 2023;1–15. doi: 10.1080/10407782.2023.2251093.
[40] Cui J, Jan A, Farooq U, Hussain M, Khan WA. Thermal analysis of radiative Darcy-Forchheimer nanofluid flow across an inclined stretching surface. Nanomaterials. 2022;12:4291. doi: 10.3390/nano12234291.
[41] Cui, J, Farooq U, Jan A, Elbashir MK, Khan WA, Mohammed M, et al. Significance of nonsimilar numerical simulations in forced convection from stretching cylinder subjected to external magnetized flow of Sisko fluid. J Maths. 2021;9540195:1–11. doi: 10.1155/2021/9540195.
[42] Tayebi T. Analysis of the local non-equilibria on the heat transfer and entropy generation during thermal natural convection in a non-Darcy porous medium. Int Commun Heat Mass Transf. 2022;135:106133. doi: 10.1016/j.icheatmasstransfer.2022.106133.
[43] Malekshah EH, Tayebi T, Sajadi SM, Jalili B, Jalili P, Aybar HS. Optimizing geometrical structure of a residential parabolic solar collector relying on hydrothermal assessment and second law analysis. Eng Anal Bound Elem. 2023;157:314–25. doi: 10.1016/j.enganabound.2023.09.011.
[44] Muhammad F, Tayebi T, Ali K, Malekshah EH, Ahmad S. Interaction of nanoparticles with motile gyrotactic microorganisms in a Darcy-Forchheimer magnetohydrodynamic flow-A numerical study. Heliyon. 2023;9(7):E17840. doi: 10.1016/j.heliyon.2023.e17840.
[45] Izadi M, Tayebi T, Alshehri HM, Hajjar A, Ben Hamida MB, Galal AM. Transient magneto-buoyant convection of a magnetizable nanofluid inside a circle sensible storage subjected to double time-dependent thermal sources. J Therm Anal Calorim. 2023;148:8511–31. doi: 10.1007/s10973-023-12242-w.
[46] Abeer S, Alnahdi, Nasir S, Gul T. Blood-based ternary hybrid nanofluid flow-through perforated capillary for the applications of drug delivery. Waves Random Complex Media. 2022;1–19. doi: 10.1080/17455030.2022.2134607.
[47] Yaseen M, Rawat SK, Shah NA, Kumar M, Eldin SM. Ternary hybrid nanofluid flow containing gyrotactic microorganisms over three different geometries with Cattaneo–Christov model. Mathematics. 2023;11:1237. doi: 10.3390/math11051237.
[48] Cao W, Animasaun IL, Yook S-J, Oladipupo VA, Xianjun J. Simulation of the dynamics of colloidal mixture of water with various nanoparticles at different levels of partial slip: Ternary-hybrid nanofluid. Int Commun Heat Mass Trans. 2022;135:106069. doi: 10.1016/j.icheatmasstransfer.2022.106069.
[49] Noreen S, Farooq U, Waqas H, Fatima N, Alqurashi MS, Imran M, et al. Comparative study of ternary hybrid nanofluids with role of thermal radiation and Cattaneo-Christov heat flux between double rotating disks. Sci Rep. 2023;13:7795. doi: 10.1038/s41598-023-34783-8.
[50] Nabwey HA, Rashad AM, Khan WA, El-Kabeir SMM, AbdElnaem S. Heat transfer in MHD flow of Carreau ternary-hybrid nanofluid over a curved surface stretched exponentially. Front Phys. 2023;11:1212715. doi: 10.3389/fphy.2023.1212715.
[51] Mahmood Z, Khan U, Saleem S, Rafique K, Eldin SM. Numerical analysis of ternary hybrid nanofluid flow over a stagnation region of stretching/shrinking curved surface with suction and Lorentz force. J Magn Magn Mater. 2023;573:170654. doi: 10.1016/j.jmmm.2023.170654.
[52] Ali K, Ahmad S, Nisar KS, Faridi AA, Ashraf M. Simulation analysisof MHD hybrid Cu-Al_2O_3/H_2O nanofluid flow with heat generation through a porous media. Int J Energy Res. 2021;45(13):19165–79. doi: 10.1002/er.7016.
[53] Ahmad S, Ali K, Faridi AA, Ashraf M. Novel thermal aspects of hybrid nanoparticles Cu-TiO_2 in the flow of ethylene glycol. Int Commun Heat Mass Transf. 2021;129:105708. doi: 10.1016/j.icheatmasstransfer.2021.105708.
[54] Sheikholeslami M, Ghasemi A. Solidification heat transfer of nanofluid in existence of thermal radiation by means of FEM. Int J Heat Mass Transf. 2018;123:418–31.
[55] Sheikholeslami M, Ganji DD, Javed MY, Ellahi R. Effect of thermal radiation on magnetohydrodynamics nanofluid flow and heat transfer by means of two phase model. J Magn Magn Mater. 2015;374:36–43.
[56] Ahmad S, Ali K, Ashraf M. MHD flow of Cu-Al_2O_3/water hybrid nanofluid through a porous media. J Porous Media. 2021;24(7):61–73. doi: 10.1615/JPorMedia.2021036704.
[57] Ahmad S, Ali K, Rizwan M, Ashraf M. Heat and mass transfer attributes of Copper-Aluminum oxide hybrid nanoparticles flow through a porous medium. Case Stud. Therm Eng. 2021;25:100932. doi: 10.1016/j.csite.2021.100932.
[58] Michael I, Yanovsky VV, Anusha T, Mahabaleshwar US. MHD flow and heat transfer of a ternary hybrid ferrofluid over a stretching/shrinking porous sheet with the effects of Brownian diffusion and thermophoresis. East Eur J Phys. 2023;1:7–18. doi: 10.26565/2312-4334-2023-1-01.
[59] Yashkun U, Zaimi K, Abu Bakar NA, Ishak A, Pop I. MHD hybrid nanofluid flow over a permeable stretching/shrinking sheet with thermal radiation effect. Int J Numer Method H. 2020;31:1014–31. doi: 10.1108/HFF-02-2020-0083.
[60] Devi SPA, Devi SSU. Numerical investigation of hydromagnetic hybrid Cu-Al_2O_3/water nanofluid flow over a permeable stretching sheet with suction. Int J Nonlinear Sci Numer Simul. 2016;17(5):249–57.
[61] Ahmad S, Ali K, Ashraf M, Khalifa HAEW, ElSeabee FAA, Tag El Din ESM. Analysis of pure nanofluid (GO/engine oil) and hybrid nanofluid (GO–Fe_3O_4/engine oil): Novel thermal and magnetic features. Nanotechnol Rev. 2022;11:2903–15.
[62] Khan WA, Pop I. Boundary-layer flow of a nanofluid past a stretching sheet. Int J Heat Mass Transf. 2010;53:2477–83.
[63] Ahmad S, Ashraf M, Ali K. Simulation of thermal radiation in a micropolar fluid flow through a porous medium between channel walls. J Therm Anal Calorim. 2021;144(3):941–53. doi: 10.1007/s10973-020-09542-w.
[64] Ahmad S, Ashraf M, Ali K. Numerical simulation of viscous dissipation in a micropolar fluid flow through a porous medium. J Appl Mech Techn Phys. 2019;60(6):996–1004. doi: 10.1134/S0021894419060038.
[65] Shahzad H, Wang X, Ghaffari A, Iqbal K, Hafeez MB, Krawczuk M, et al. Fluid structure interaction study of non-Newtonian Casson fluid in a bifurcated channel having stenosis with elastic walls. Sci Rep. 2022;12:12219. doi: 10.1038/s41598-022-16213-3.
[66] Hafeez MB, Krawczuk M, Shahzad H, Pasha AA, Adil M. Simulation of hybridized nanofluids flowing and heat transfer enhancement via 3-D vertical heated plate using finite element technique. Sci Rep. 2022;12:11658. doi: 10.1038/s41598-022-15560-5.
[67] Shahzad H, Ain QU, Pasha AA, Irshad K, Shah IA, Ghaffari A, et al. Double-diffusive natural convection energy transfer in magnetically influenced Casson fluid flow in trapezoidal enclosure with fillets. Int Commun Heat Mass Transf. 2022;137:106236. doi: 10.1016/j.icheatmasstransfer.2022.106236.
[68] Tayebi T, El-Sapa S, Karimi N, Dogonchi AS, Chamkha AJ, Galal AM. Double-diffusive natural convection with Soret/Dufour effects and

energy optimization of nano-encapsulated phase change material in a novel form of a wavy-walled I-shaped domain. J Taiwan Inst Chem Eng. 2023;148:104873. doi: 10.1016/j.jtice.2023.104873.
[69] Pasha AA, Tayebi T, MottahirAlam M, Irshad K, Dogonchi AS, Chamkha AJ, et al. Efficacy of exothermic reaction on the thermal-free convection in a nano-encapsulated phase change materials-loaded enclosure with circular cylinders inside. J Energy Storage. 2023;59:106522. doi: 10.1016/j.est.2022.106522.
[70] Alsabery AI, Vaezi M, Tayebi T, Hashim I, Ghalambaz M, Chamkha AJ. Nanofluid mixed convection inside wavy cavity with heat source: A non-homogeneous study. Case Stud Therm Eng. 2022;34:102049. doi: 10.1016/j.csite.2022.102049.
[71] Amin R, Alrabaiah H, Hafeez MB. A computational algorithm for the numerical solution of nonlinear fractional integral equations. Fractals. 2022;30(1):2240030. doi: 10.1142/S0218348X22400308.
[72] Amin R, Sitthiwirattham T, Hafeez MB, Sumelka W. Haar collocations method for nonlinear variable order fractional integro-differential equations. Progr Fract Differ Appl. 2023;9(2):223–9.
[73] Farooq J, Mushtaq M, Munir S, Ramzan M, Chung JD, Farooq U. Slip flow through a non-uniform channel under the influence of transverse magnetic field. Sci Rep. 2018;8:13137. doi: 10.1038/s41598-018-31538-8.
[74] Razzaq R, Farooq U, Cui J, Muhammad T. Non-similar solution for magnetized flow of maxwell nanofluid over an exponentially stretching surface. Math Probl Eng. 2021;2021:5539542–10. doi: 10.1155/2021/5539542.
[75] Razzaq R, Farooq U. Non-similar forced convection analysis of Oldroyd-B fluid flow over an exponentially stretching surface. Adv Mech Eng. 2021;13(7):168781402110346. doi: 10.1177/16878140211034604.
[76] Cui J, Munir S, Raies SF, Farooq U, Razzaq R. Non-similar aspects of heat generation in bioconvection from flat surface subjected to chemically reactive stagnation point flow of Oldroyd-B fluid. Alex Eng J. 2022;61(7):5397–411. doi: 10.1016/j.aej.2021.10.056.